JYX

JYVÄSKYLÄN YLIOPISTO
UNIVERSITY OF JYVÄSKYLÄ

This is a self-archived version of an original article. This version may differ from the original in pagination and typographic details.

Author(s): Hummelshøj, J. S.; Landis, D. D.; Voss, J; Jiang, T.; Tekin, A; Bork, N.; Dułak, M.; Mortensen, J. J.; Adamska, L.; Andersin, J.; Baran, J. D.; Barmparis, G. D.; Bell, F.; Bezanilla, A. L.; Bjork, J.; Björketun, M. E.; Bleken, F.; Buchter, F.; Bürkle, M.; Burton, P. D.; Buus, B. B.; Calborean, A.; Calle-Vallejo, F.; Casolo, S.; Chandler, B. D.; Chi, D. H.; Czekaj, I.; Datta, S.; Datye, A.; DeLaRiva, A.; Despoja, V.; Dobrin, S.;

Title: DFT based screening of ternary alkali-transition metal borohydrides : a computational materials design project

Year: 2009

Version: Published version

Please cite the original version:

Hummelshøj, J. S., Landis, D.D., Voss, J., Jiang, T., Tekin, A., Bork, N., Dułak, M., Mortensen, J.J., Adamska, L., Andersin, J., Baran, J. D., Barmparis, G. D., Bell, F., Bezanilla, A. L., Bjork, J., Björketun, M. E., Bleken, F., Buchter, F., Bürkle, M., . . . Vegge, T. (2009). DFT based screening of ternary alkali-transition metal borohydrides : a computational materials design project. Journal of Chemical Physics, 131(1), Article 014101. https://doi.org/10.1063/1.3148892

Density functional theory based screening of ternary alkali-transition metal borohydrides: A computational material design project

J. S. Hummelshøj; D. D. Landis; J. Voss; T. Jiang; A. Tekin; N. Bork; M. Dułak; J. J. Mortensen; L. Adamska; J. Andersin; J. D. Baran; G. D. Barmparis; F. Bell; A. L. Bezanilla; J. Bjork; M. E. Björketun; F. Bleken; F. Buchter; M. Bürkle; P. D. Burton; B. B. Buus; A. Calborean; F. Calle-Vallejo; S. Casolo; B. D. Chandler; D. H. Chi; I Czekaj; S. Datta; A. Datye; A. DeLaRiva; V Despoja; S. Dobrin; M. Engelund; L. Ferrighi; P. Frondelius; Q. Fu; A. Fuentes; J. Fürst; A. García-Fuente; J. Gavnholt; R. Goeke; S. Gudmundsdottir; K. D. Hammond; H. A. Hansen; D. Hibbitts; E. Hobi, Jr.; J. G. Howalt; S. L. Hruby; A. Huth; L. Isaeva; J. Jelic; I. J. T. Jensen; K. A. Kacprzak; A. Kelkkanen; D. Kelsey; D. S. Kesanakurthi; J. Kleis; P. J. Klüpfel; I Konstantinov; R. Korytar; P. Koskinen; C. Krishna; E. Kunkes; A. H. Larsen; J. M. G. Lastra; H. Lin; O. Lopez-Acevedo; M. Mantega; J. I. Martínez; I. N. Mesa; D. J. Mowbray; J. S. G. Mýrdal; Y. Natanzon; A. Nistor; T. Olsen; H. Park; L. S. Pedroza; V Petzold; C. Plaisance; J. A. Rasmussen; H. Ren; M. Rizzi; A. S. Ronco; C. Rostgaard; S. Saadi; L. A. Salguero; E. J. G. Santos; A. L. Schoenhalz; J. Shen; M. Smedemand; O. J. Stausholm-Møller; M. Stibius; M. Strange; H. B. Su; B. Temel; A. Toftelund; V Tripkovic; M. Vanin; V Viswanathan; A. Vojvodic; S. Wang; J. Wellendorff; K. S. Thygesen; J. Rossmeisl; T. Bligaard; K. W. Jacobsen; J. K. Nørskov; T. Vegge

Check for updates

View Online   Export Citation

Articles You May Be Interested In

Ni-induced destabilization dynamics of crystalline zinc borohydride

Appl. Phys. Lett. (April 2008)

Simultaneous desorption behavior of M borohydrides and Mg_2FeH_6 reactive hydride composites (M = Mg, then Li, Na, K, Ca)

Appl. Phys. Lett. (August 2015)

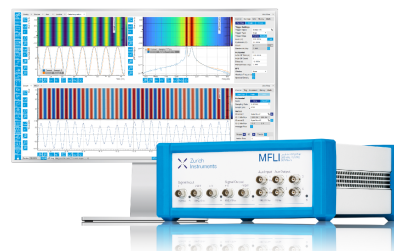Chemical bonding analysis on amphoteric hydrogen – alkaline earth ammine borohydrides

AIP Conference Proceedings (April 2018)

Density functional theory based screening of ternary alkali-transition metal borohydrides: A computational material design project

J. S. Hummelshøj, D. D. Landis, J. Voss, T. Jiang, A. Tekin, N. Bork, M. Dułak,
J. J. Mortensen, L. Adamska, J. Andersin, J. D. Baran, G. D. Barmparis, F. Bell,
A. L. Bezanilla, J. Bjork, M. E. Björketun, F. Bleken, F. Buchter, M. Bürkle, P. D. Burton,
B. B. Buus, A. Calborean, F. Calle-Vallejo, S. Casolo, B. D. Chandler, D. H. Chi,
I Czekaj, S. Datta, A. Datye, A. DeLaRiva, V Despoja, S. Dobrin, M. Engelund, L. Ferrighi,
P. Frondelius, Q. Fu, A. Fuentes, J. Fürst, A. García-Fuente, J. Gavnholt, R. Goeke,
S. Gudmundsdottir, K. D. Hammond, H. A. Hansen, D. Hibbitts, E. Hobi, Jr., J. G. Howalt,
S. L. Hruby, A. Huth, L. Isaeva, J. Jelic, I. J. T. Jensen, K. A. Kacprzak, A. Kelkkanen,
D. Kelsey, D. S. Kesanakurthi, J. Kleis, P. J. Klüpfel, I Konstantinov, R. Korytar,
P. Koskinen, C. Krishna, E. Kunkes, A. H. Larsen, J. M. G. Lastra, H. Lin,
O. Lopez-Acevedo, M. Mantega, J. I. Martínez, I. N. Mesa, D. J. Mowbray, J. S. G. Mýrdal,
Y. Natanzon, A. Nistor, T. Olsen, H. Park, L. S. Pedroza, V Petzold, C. Plaisance,
J. A. Rasmussen, H. Ren, M. Rizzi, A. S. Ronco, C. Rostgaard, S. Saadi, L. A. Salguero,
E. J. G. Santos, A. L. Schoenhalz, J. Shen, M. Smedemand, O. J. Stausholm-Møller,
M. Stibius, M. Strange, H. B. Su, B. Temel, A. Toftelund, V Tripkovic, M. Vanin,
V Viswanathan, A. Vojvodic, S. Wang, J. Wellendorff, K. S. Thygesen, J. Rossmeisl,
T. Bligaard, K. W. Jacobsen, J. K. Nørskov, and T. Vegge[a)]
*The 2008 CAMD Summer School in Electronic Structure Theory and Materials Design, Center
for Atomic-scale Materials Design, Department of Physics, Technical University of Denmark,
DK-2800 Kgs. Lyngby, Denmark*[b)]

We present a computational screening study of ternary metal borohydrides for reversible hydrogen storage based on density functional theory. We investigate the stability and decomposition of alloys containing 1 alkali metal atom, Li, Na, or K (M_1); and 1 alkali, alkaline earth or $3d/4d$ transition metal atom (M_2) plus two to five $(BH_4)^-$ groups, i.e., $M_1M_2(BH_4)_{2-5}$, using a number of model structures with trigonal, tetrahedral, octahedral, and free coordination of the metal borohydride complexes. Of the over 700 investigated structures, about 20 were predicted to form potentially stable alloys with promising decomposition energies. The $M_1(Al/Mn/Fe)(BH_4)_4$, $(Li/Na)Zn(BH_4)_3$, and $(Na/K)(Ni/Co)(BH_4)_3$ alloys are found to be the most promising, followed by selected $M_1(Nb/Rh)(BH_4)_4$ alloys. © *2009 American Institute of Physics.*
[DOI: 10.1063/1.3148892]

I. INTRODUCTION

The development of sustainable energy solutions for the future requires new and improved materials. Specifically designed material properties are needed to solve the grand challenges in energy production, storage, and conversion. Within energy storage, hydrogen has been investigated extensively over the past decade[1] as one of the few promising energy carriers which can provide a high energy density without resulting in CO_2 emission by the end user. Finding materials for efficient, reversible hydrogen storage, however, remains challenging. Here, the specific requirements of the rapidly growing transportation sector coupled with complex engineering challenges[2] have directed research toward complex materials with extreme hydrogen storage capacities[3] such as metal borohydrides[4] and metal ammines.[5] Finding materials with high reversible hydrogen content and optimal thermodynamic stability is essential if hydrogen is going to be used

as a commercial fuel in the transport sector. The binary metal borohydrides have been studied extensively: the alkali based compounds, e.g., $LiBH_4$,[6–8] are too thermodynamically stable, the alkaline earth compounds are kinetically too slow and practically irreversible,[9] and the transition metal borohydrides are either unstable or irreversible.[10] This leaves hope that mixed metal ("alloyed") systems might provide new opportunities.

The use of computational screening techniques has proved a valuable tool in narrowing the phase space of potential candidate materials for hydrogen storage.[11,12] Recent density functional theory (DFT) calculations have shown that the thermodynamic properties of even highly complex borohydride superstructures can be estimated by DFT using simple model structures, if the primary coordination polyhedra are correctly accounted for.[13] These findings enable faster screening studies of thermodynamic stability and decomposition temperatures for, e.g., ternary and quaternary borohydride systems; not only in terms of reduced computational effort due to smaller system sizes but also with the advantage that the exact space group does not need to be known

---

a priori.

In the present paper, we apply a "local coordination screening" (LCS) approach to search for novel metal borohydrides. The vast majority of the calculations were performed as part of the 2008 CAMD summer school in electronic structure theory and materials design, where more than 100 scientists combined DFT calculations, database methods, and screening techniques to investigate the structure and stability of promising ternary borohydrides. A few additional calculations were subsequently performed based on the insight gained from the initial screening.

Out of 757 investigated $M_1M_2(BH_4)_{2-5}$ (M_1=alkali metal and M_2=alkali, alkaline earth or $3d/4d$ transition metal) compositions and structures, a total of 22 were found to form potentially stable alloys with promising decomposition energies, which should subsequently be subjected to more detailed theoretical and experimental verification.

II. COMPUTATIONAL SETUP

Groups of alloy compositions and structures were divided among different groups of scientists, each of which was responsible for its own subset of the alloy configuration space. A number of predefined structural templates and optimization procedures had been prepared to assist the groups in setting up structures and calculations for the initial optimization (see Sec. II B). This was done to ensure a sufficient accuracy in all calculations (i.e., convergence with respect to plane wave cutoff, k-point sampling, etc.).

To ensure reliability of the generated results, an automated checking procedure was enforced before a result could be included in the database (see Sec. III) to ensure the presence of the required output (total energies, lattice constants, etc.).

A. Computational parameters

The total energies and gradients were calculated within density functional theory[14] as implemented by the software package Dacapo.[15] A plane wave basis set with a cutoff energy of 350 eV (density grid cutoff of 700 eV) and the RPBE exchange-correlation functional[15] were used for all calculations. Dacapo uses ultrasoft pseudopotentials[16] for a description of the ionic cores. The coordinate optimization was implemented and performed within the atomic simulation environment.[17] The electronic Brillouin zones were sampled with ($4 \times 4 \times 4$) k-points (spacings of ~ 0.05 Å^{-1}). A quasi-Newton method[18] was used for all relaxations.

B. Configuration space and template structures

The alloys which were initially screened have the general formula $M_1M_2(BH_4)_x$, where $M_1 \in \{Li, Na, K\}$ and $x=2-4$. The $x=2$ alloys were investigated for $M_2 \in \{Li, Na, K\}$, and $x=3,4$ for $M_2 \in \{Li, Na, K, Mg, Al, Ca, Sc-Zn, Y-Mo, Ru-Cd\}$.

In order to limit the total number of calculations, only template structures with tetrahedral and octahedral coordination of the $(BH_4)^-$ groups to the metal atoms were used. Most metals prefer an octahedral coordination of their ligands, but for the metal borohydrides the ligand-ligand re-

pulsion between the relatively large $(BH_4)^-$ ions often forces a lower coordination number. The primary structures observed and reported in literature for the alkali and alkaline earth borohydrides are either tetrahedral (for the smallest Li and Mg) or octahedral (for the larger Na, K, and Ca), while a trigonal planar ligand arrangement is observed for $Al(BH_4)_3$. However, Al can also have a tetrahedral coordination as is the case of the $LiAl(BH_4)_4$ alloy obtained here (see Sec. V), and since the radii of the considered ions lie between the radius for K and the radius for Al, the tetrahedral and octahedral primary structures are expected to be representative.

For each alloy composition, four different template structures were used to sample the tetrahedral and octahedral primary structures in the combinations: tetrahedral/tetrahedral, octahedral/octahedral, tetrahedral/octahedral, and octahedral/tetrahedral, referring to the coordination of the $(BH_4)^-$ groups to the M_1 and M_2 atoms, respectively. The coordination polyhedra were either corner sharing, edge sharing, or a combination to yield the required stoichiometric ratio of $(BH_4)^-$ groups (see Fig. 1). All structures were designed to have a unit cell containing only one formula unit (see Sec. II D). It has previously been shown that these simple template structures can be within ~ 0.1 eV (10 kJ/mol H_2) of the true ground state energy if the local coordination is correctly accounted for; e.g., $M_1M_2(BH_4)_2$-tetra for $LiBH_4$,[7] $M_1M_2(BH_4)_4$-octa for $Ca(BH_4)_2$,[19] and even $M_1M_2(BH_4)_4$-tetra for the free energy of $Mg(BH_4)_2$ superstructures.[13]

The initial optimization of the structures only relaxed the hydrogen positions and the unit cell volume while keeping the metal-boron coordination polyhedra fixed. For a given set of (M_1, M_2), the most stable structure was then used as the starting point for a calculation in which all atomic positions and the unit cell were relaxed. Even though many of the structures did not change significantly during the final relaxation, it added, in principle, an additional structure to the phase space for each set of (M_1, M_2). These are included as "other" structures in the results (Figs. 3–12) to distinguish them from the structures with fixed metal-boron coordination polyhedra, even though the original coordination polyhedra are only slightly distorted in many of them.

A number of structures were subsequently added based on the knowledge gained from the initial screening and the reference binary borohydride structures (see Secs. IV and VI). In some of these structures, the metal ions had the same valence as in the reference structures, which meant that the four $x=2$ templates were also applied to $M_2 \in \{Ni, Pd, Cu, Ag\}$, while a new template for $x=5$ was investigated for $M_2 \in \{Ti, Zr\}$ in the two combinations tetrahedral/octahedral and octahedral/tetrahedral. An alternative $x=3$ tetragonal/trigonal template was applied to $M_2 \in \{Mg, Al, Ca, Sc-Zn, Y-Mo, Ru-Cd\}$ to investigate possible size effects. In this structure, the M_1 ion has a tetrahedral coordination while the M_2 atom is surrounded by three $(BH_4)^-$ groups in a trigonal planar arrangement (see Fig. 2). This enabled the metal-boron distances for the two metals to be optimized independently, which was not pos-
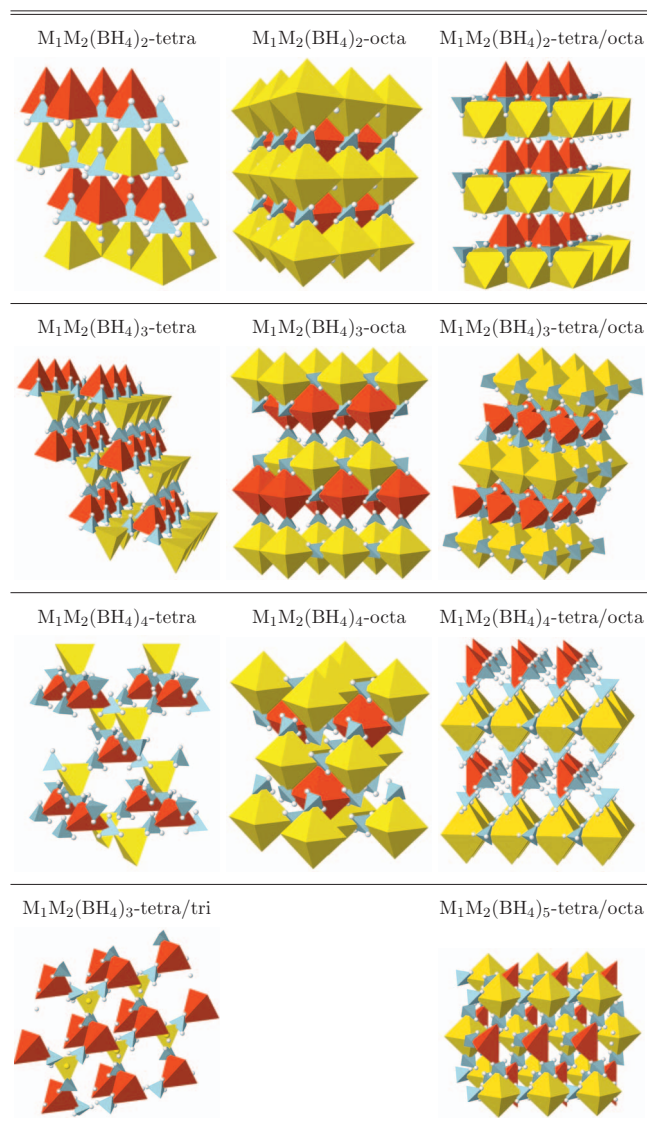
FIG. 1. The template structures of $M_1M_2(BH_4)_{2-5}$. Red and yellow polyhedra show the coordination of the B atoms around the M_1 and M_2 atoms, respectively; blue tetrahedra represent the $(BH_4)^-$ groups. The octa/tetra structures are obtained by switching M_1 and M_2 in the tetra/octa structures.

sible in the original $x=3$ templates, but found to be required to obtain the preferred local coordination of certain alloys.

In total, 757 structures have been simulated and are reported herein.

C. Group calculations

The 69 sets of (M_1, M_2) combinations investigated in this study were divided among 32 groups of scientists for the initial screening. Each group followed step I of the calculational procedure outlined below for each alloy containing M_1 and M_2 and step II for the most stable resulting structure.

D. Calculational procedure

1. Step I

An initial structure was set up by calling a function that populates one of the four template structures with two supplied metal ions, e.g., Li and Sc. The function utilizes the

TABLE I. The calculated reference energies for the binary borohydrides in their most stable template structures (see Fig. 2).

	wt % (kg H$_2$/kg material)	ΔE_{decomp} (eV/H$_2$)
K(BH$_4$)	7.5	−0.968
Na(BH$_4$)	10.7	−0.729
Li(BH$_4$)	18.5	−0.422
Ag(BH$_4$)	3.3	0.278
Cu(BH$_4$)	5.1	0.352
Pd(BH$_4$)	3.3	0.661
Ni(BH$_4$)	5.5	0.680
Ca(BH$_4$)$_2$	11.6	−0.636
Mg(BH$_4$)$_2$	14.9	−0.467
Zn(BH$_4$)$_2$	8.5	−0.063
Cd(BH$_4$)$_2$	5.7	−0.043
V(BH$_4$)$_2$	10.0	−0.031
Nb(BH$_4$)$_2$	6.6	0.066
Fe(BH$_4$)$_2$	9.4	0.090
Cr(BH$_4$)$_2$	9.9	0.162
Mn(BH$_4$)$_2$	9.5	0.174
Co(BH$_4$)$_2$	9.1	0.264
Mo(BH$_4$)$_2$	6.4	0.280
Rh(BH$_4$)$_2$	6.1	0.340
Ru(BH$_4$)$_2$	6.2	0.351
Y(BH$_4$)$_3$	9.1	−0.676
Sc(BH$_4$)$_3$	13.5	−0.595
Al(BH$_4$)$_3$	16.9	−0.209
Zr(BH$_4$)$_4$	10.7	−0.429
Ti(BH$_4$)$_4$	15.0	−0.252

ionic radii obtained from the calculations of binary reference borohydrides, i.e., individual metal atom borohydrides, to calculate metal-boron distances, where the ionic radius used for a $(BH_4)^-$ group depends on whether a face, edge or corner of the H-tetrahedron points toward the metal atom. In general, this ensured that the effective lattice constant and the c/a ratio were close to the optimum. The initial structure was used as the initial guess for the first iteration of the following procedure.

All hydrogen positions were relaxed until the maximum force on the atoms reached 0.05 eV/Å or, alternatively, a maximum of 50 quasi-Newton steps had been performed. The resulting structure was then contracted and expanded to 90%, 95%, 105%, and 110% of the unit cell volume by a proportional scaling of the unit cell, while keeping the B–H distances in each $(BH_4)^-$ group fixed; a single total energy calculation was performed for each volume. A Murnaghan equation-of-state was fitted to the calculated five points to estimate the optimal unit cell volume, to which the unit cell was then scaled (again while conserving B–H distances), followed by a relaxation of the hydrogen positions to a force convergence of 0.05 eV/Å.

After each iteration, an energy versus unit cell volume plot was inspected visually to decide whether the minimum had been sufficiently sampled or an additional iteration of the procedure should be performed; in the latter case, a structure resulting from the first iteration was used as the starting guess for the next iteration.
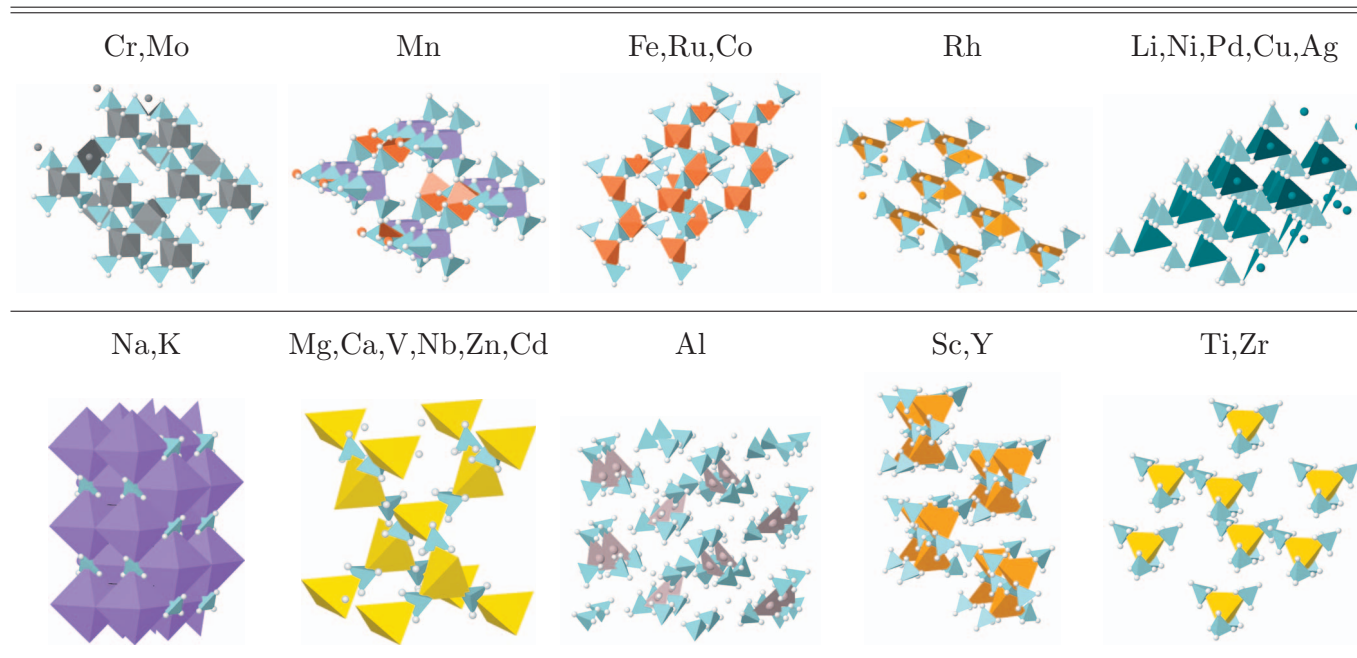
FIG. 2. The structures used for calculating the binary reference energies. For Cr, Mo, Mn, Fe, Ru, Co, Rh, Li, Ni, Pd, Cu, and Ag, the polyhedra show the coordination of the H atoms; the coordination of the $(BH_4)^-$ groups are tetrahedral in these structures. For the remaining metals the coordination polyhedra show the coordination of the $(BH_4)^-$ groups.

2. Step II

When all template structures for each of the (M_1, M_2) alloys had been optimized in step I, the most stable structure was relaxed without constraints by repeating the procedure that first relaxes all atomic positions for a fixed cell and then the unit cell for fixed internal positions. To limit the computational time used by this algorithm, the number of iterations was limited to 5, and the number of steps per iteration was limited to 12 for the internal relaxation and 5 for the unit cell relaxation.

3. Procedure for the additional structures

For the structures calculated later, the $x=2$ structures (monovalent transition metals) followed the same procedure mentioned above, whereas only a single free optimization was performed on the extra $x=3$ and $x=5$ structures, in which all atoms were allowed to relax.

III. DATA COLLECTION AND STORAGE

Every group executed the calculation procedures for steps I and II. After each step, the validity of the results was checked by the group and the results were checked in (stored in a global location for indexing) to the common database.

A. Front end

A Python[20] script took care of checking in all relevant files that were needed for subsequent checking. This included the calculation script and the output files containing the atoms, energies and the calculational parameters. A subversion (svn) version control system[21] assisted to manage groups and users, storing results and assuring transaction consistency.

B. Back end

A second Python script was used to extract the relevant parameters, i.e., the total energy, unit cell volume, chemical symbols, structure, and the calculational parameters such as k-points, number of bands, density wave cutoff, and to select the best structure (at any given time) for every borohydride to create/update the intermediate result plots, which were accessible to all participants. Python, in combination with Matplotlib,[22] was used to ensure a flexible user interface and to generate the plots. A special Python class managed the resulting data, consisting of approximately 5500 calculations. This class provided basic database operations such as selecting, sorting, and filtering of data and facilitated the creation of the plots considerably.

The overall construction of the database and data retrieval procedures will also facilitate screening for possible correlations between combinations of a number of different values in future projects.

IV. DATA ANALYSIS

The initial screening procedure presented here is performed to reduce the number of potential alloys for further investigation, and two simple selection criteria were set up to assess the stability of the investigated alloy structures against phase separation/disproportionation and decomposition. The stabilities were first analyzed against phase separation into the original binary borohydrides as illustrated for $LiSc(BH_4)_4$:

$$\Delta E_{\text{alloy}} = E_{\text{LiSc(BH}_4)_4} - (E_{\text{LiBH}_4} + E_{\text{Sc(BH}_4)_3}). \quad (1)$$

Reference energies for the 3 alkali, 2 alkaline earth, $Al(BH_4)_3$ plus 19 transition metal borohydrides were ob-

TABLE II. Structures with alloying energies $\Delta E_{\text{alloy}} < 0.0$ eV/f.u. (formula unit) and decomposition energies $\Delta E_{\text{decomp}} < 0.0$ eV/H$_2$.

	wt % (kg H$_2$/kg material)	ΔE_{alloy} (eV/f.u.)	ΔE_{decomp} (eV/H$_2$)
LiNa(BH$_4$)$_2$	13.5	−0.020	−0.581
KZn(BH$_4$)$_3$	8.1	−0.349	−0.423
KAl(BH$_4$)$_4$	12.9	−0.138	−0.416
NaAl(BH$_4$)$_4$	14.7	−0.279	−0.373
KCd(BH$_4$)$_3$	6.2	−0.005	−0.352
NaZn(BH$_4$)$_3$	9.1	−0.358	−0.344
LiAl(BH$_4$)$_4$	17.3	−0.391	−0.311
KFe(BH$_4$)$_3$	8.7	−0.116	−0.282
LiZn(BH$_4$)$_3$	10.4	−0.362	−0.243
NaFe(BH$_4$)$_3$	9.8	−0.141	−0.206
KMn(BH$_4$)$_4$	10.5	−0.148	−0.174
NaNb(BH$_4$)$_4$	9.2	−0.128	−0.165
KCo(BH$_4$)$_3$	8.5	−0.089	−0.161
NaMn(BH$_4$)$_4$	11.7	−0.284	−0.131
KNi(BH$_4$)$_3$	8.5	−0.120	−0.116
LiFe(BH$_4$)$_3$	11.3	−0.141	−0.104
LiNb(BH$_4$)$_4$	10.1	−0.194	−0.097
NaCo(BH$_4$)$_3$	9.6	−0.143	−0.090
KRh(BH$_4$)$_4$	8.0	−0.058	−0.079
LiMn(BH$_4$)$_4$	13.3	−0.358	−0.063
NaNi(BH$_4$)$_3$	9.6	−0.164	−0.043
NaRh(BH$_4$)$_4$	8.7	−0.033	−0.016

TABLE III. Structures with alloying energies $0 < \Delta E_{\text{alloy}} < 0.2$ eV/f.u. (formula unit) with decomposition energies $\Delta E_{\text{decomp}} < 0.0$ eV/H$_2$.

	wt % (kg H$_2$/kg material)	ΔE_{alloy} (eV/f.u.)	ΔE_{decomp} (eV/H$_2$)
KNa(BH$_4$)$_2$	8.8	0.095	−0.825
NaY(BH$_4$)$_4$	9.4	0.115	−0.675
NaCa(BH$_4$)$_3$	11.2	0.129	−0.645
LiY(BH$_4$)$_4$	10.4	0.033	−0.609
LiCa(BH$_4$)$_3$	13.2	0.052	−0.556
LiSc(BH$_4$)$_4$	14.5	0.143	−0.534
NaCd(BH$_4$)$_3$	6.7	0.003	−0.271
KNb(BH$_4$)$_4$	8.4	0.016	−0.207
NaV(BH$_4$)$_4$	12.1	0.076	−0.188
NaAg(BH$_4$)$_2$	5.0	0.193	−0.177
LiCd(BH$_4$)$_3$	7.4	0.102	−0.152
KCr(BH$_4$)$_4$	10.7	0.199	−0.136
LiV(BH$_4$)$_4$	13.8	0.061	−0.113
NaCr(BH$_4$)$_4$	12.0	0.050	−0.095
KPd(BH$_4$)$_3$	6.4	0.047	−0.095
KMo(BH$_4$)$_4$	8.3	0.185	−0.079
KRu(BH$_4$)$_3$	6.5	0.168	−0.061
NaMo(BH$_4$)$_4$	9.0	0.056	−0.035
LiCr(BH$_4$)$_4$	13.6	0.029	−0.021
NaPd(BH$_4$)$_3$	7.0	0.052	−0.014

$$\Delta E_{\text{decomp}} = E_{\text{LiMn(BH}_4)_3} - (E_{\text{LiH}} + E_{\text{Mn}} + 3E_{\text{B}} + 5.5E_{\text{H}_2}).$$

(2)

In this definition, ΔE_{decomp} estimates the stability of the alloy against decomposition. Transition metal hydrides, metal borides, higher order boranates and diborane, which may potentially form, are thus not taken into consideration in this first screening.

The analysis is based on the ground state energies only. Although the difference in vibrational entropy between hydrogen in an alkali metal borohydride and in the gas phase is often significantly smaller than in conventional metal hydrides,[31] the contributions to the free energy from the vibrational entropy may be significant.

A stability range of $\Delta E_{\text{alloy}} \leq 0.0$ eV/f.u. (formula unit) and $\Delta E_{\text{decomp}} \in \{-0.5; 0.0\}$ eV/H$_2$ is used to select the most interesting alloys with $\Delta E_{\text{decomp}} = -0.2$ eV/H$_2$ as the target value (see Table II), but given the idealized screening criteria in Eqs. (1) and (2), alloys with only small instabilities, i.e., $\Delta E_{\text{alloy}} \leq 0.2$ eV/f.u and $\Delta E_{\text{decomp}} \leq 0.0$ eV/H$_2$ should not be discarded *a priori* (see Table III).

V. RESULTS

As the first step of the stability screening, we have plotted the alloying energy against the decomposition energy of the 757 investigated alloys (see Fig. 3). Most of the alloys are found to be stable against decomposition, but the majority are found to be unstable against separation into their binary components ($\Delta E_{\text{alloy}} > 0.0$ eV/f.u.). Many are still within the 0.2 eV/f.u. boundary regime. The lithium-containing alloys (red) are less stable against decomposition than those containing sodium (blue) and potassium (green). Restricting the plot to only the most stable structure for each

tained using the most stable structures among the applied $M_2(\text{BH}_4)_{1-4}$ model templates (see Table I). Due to computational constraints, the performed calculations are not spin polarized, which causes certain reference structures, e.g., Mn(BH$_4$)$_2$, to become unstable. In order not to exclude potentially stable candidates, the assessment in Eq. (1) was used for all reference structures (see Table I).

For assessing the stability of alloys with a potentially less favorable stoichiometry, like LiSc(BH$_4$)$_3$, an effective reference value for $E_{\text{Sc(BH}_4)_2}$ was determined from the stable $E_{\text{Sc(BH}_4)_3}$ as $E_{\text{Sc(BH}_4)_2}* = E_{\text{Sc(BH}_4)_3} - 2E_{\text{H}_2} - E_{\text{B}}$. Using $1/2(\text{B}_2\text{H}_6 + \text{H}_2)$ as a reference only shifts the energy by 0.07 eV/H$_2$ and does not result in a new preferred coordination for any of the stable alloys.

The decomposition pathways of binary and ternary metal borohydrides are often highly complex and differ significantly from one system to the next, e.g., LiBH$_4$,[23] Mg(BH$_4$)$_2$,[24] and LiZn(BH$_4$)$_3$,[25] and the formed products can even depend on the details of the desorption conditions. Certain compounds form transition metal hydrides,[26] others form transition metal borides,[27] di-,[10] or dodeca-boranes[28] and others again, e.g., Cr, Cd, Mn, and Zn(BH$_4$)$_2$ decompose to the elements.[29,30] Given the inclusive nature of this initial screening study and the fact that the true decomposition pathways in most of the investigated alloys are not well known, a simple and generic decomposition pathway was selected, which all interesting mixed borohydrides must be stable against (as a minimum). Here, the alloys decompose into the highly stable alkali- and alkaline earth hydrides, transition metals, boron and H$_2$, e.g.:
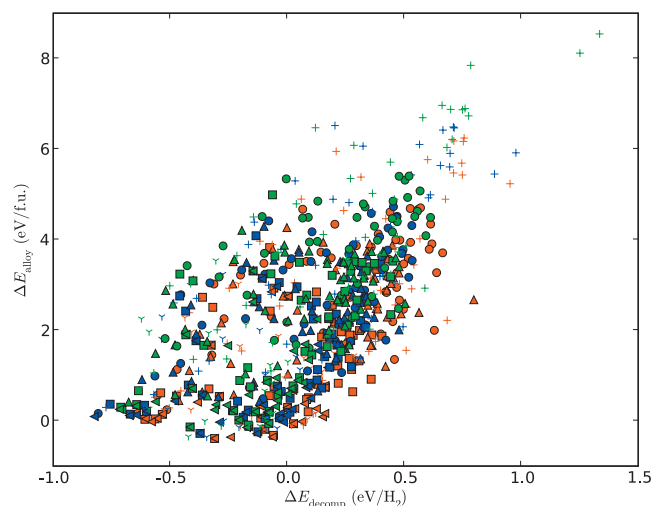
FIG. 3. The alloying energy, ΔE_{alloy}, as a function of the decomposition energy, ΔE_{decomp}, for all alloy compositions. Colors: Li (red), Na (blue), and K (green). Investigated coordinations: tetra ($\square$), octa ($\bigcirc$), octa-tetra ($\triangle$), tetra-octa (+), tetra-tri ($\curlyvee$), other ($\triangleleft$). Total number of structures: 757.

FIG. 5. The hydrogen density (kg H_2 m^{-3} as a function of the decomposition energy for the 22 alloys with $\Delta E_{alloy} \leq 0.0$ eV/f.u. and $\Delta E_{decomp} \leq 0.0$ eV/H_2. References to experimental observations: !: Ref. 25, @: Ref. 37, &: Ref. 38, *: Ref. 39. Colors: Li (red), Na (blue), and K (green). Preferred local coordination: tetra ($\square$), octa ($\bigcirc$), octa-tetra ($\triangle$), tetra-octa (+), tetra-tri ($\curlyvee$), other ($\triangleleft$).

M_1M_2 system (see Fig. 4) seems to support this observation, and yields a total of 22 stable alloys (see Table II). Figure 4 is dominated by alloys where (a) both metal atoms are tetrahedrally coordinated to the borohydride groups ($\square$), (b) one is tetrahedral the other trigonal ($\curlyvee$), and (c) so-called other ($\triangleleft$), where all constraints have been lifted. Some octa-tetra ($\triangle$) and tetra-octa (+) are also observed.

Plotting the hydrogen density of the stable alloys, $\Delta E_{alloy} \leq 0.0$ eV/f.u. and $\Delta E_{decomp} \leq 0.0$ eV/H_2, Fig. 5 shows that alloys containing potassium (in green) are found to have the lowest density, followed by sodium (in blue) and lithium (in red), as expected. The overall density is found to be around that of liquid hydrogen, which is largely due to the choice of simple template structures; higher densities are expected for real systems as previously observed for $Mg(BH_4)_2$.[9] Alloys containing Al, Mn, Fe, and Zn are found to be stable for all alkali metals screened, whereas those
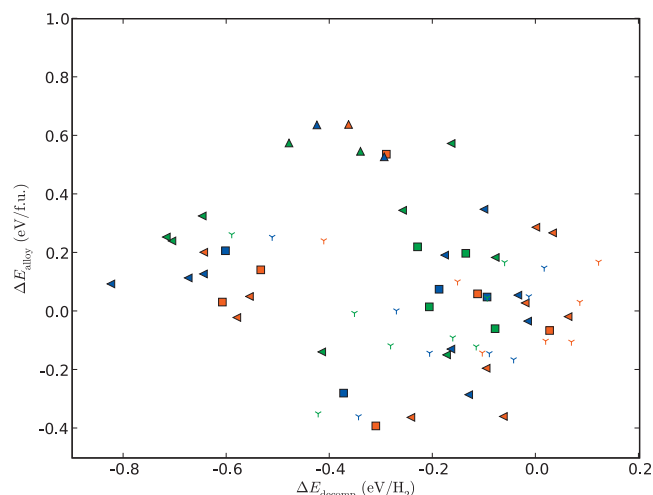
based on Co, Ni, Nb, and Rh are stable for two out of three alkali metals. The only other stable alloys are $KCd(BH_4)_3$ and $LiNa(BH_4)_2$ (see Table II).

The storage capacity (wt % hydrogen) of the stable alloys is plotted as a function of the decomposition energy, ΔE_{decomp}, in Fig. 6. Here, the data from the binary reference structures have also been included, and it is clearly seen that the stability has been reduced significantly compared to the highly stable binary borohydrides. Most alloys have storage capacities above the DOE 2015 system target of 9 wt % (Ref. 3) and several also have favorable stabilities. A number of these ternary borohydrides have been synthesized either

FIG. 4. The alloying energy, ΔE_{alloy}, as a function of the decomposition energy, ΔE_{decomp}, for all preferred alloy systems. Colors: Li (red), Na (blue) and K (green). Preferred local coordination: tetra ($\square$), octa ($\bigcirc$), octa-tetra ($\triangle$), tetra-octa (+), tetra-tri ($\curlyvee$), other ($\triangleleft$).
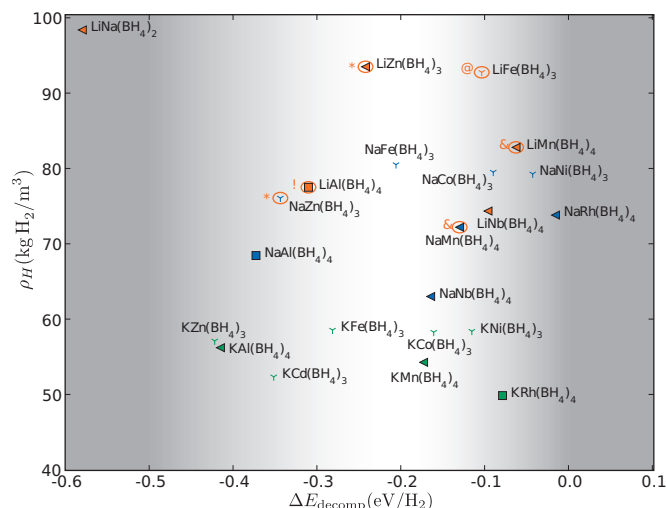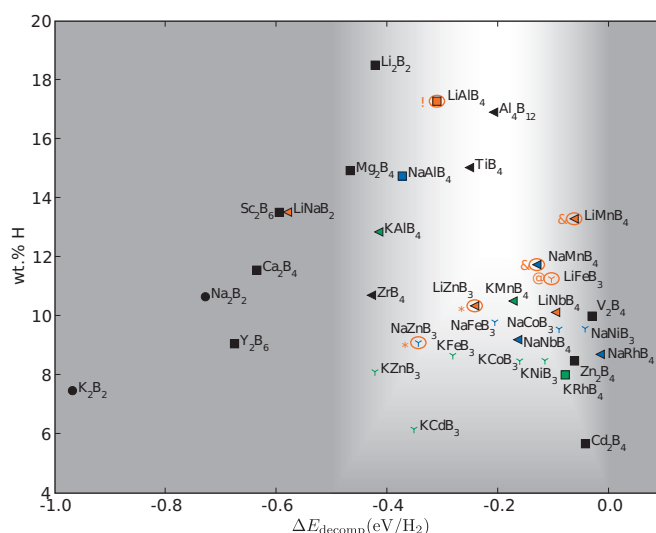

FIG. 6. The weight percent of hydrogen (wt. %) as a function of the decomposition energy, ΔE_{decomp} [Eq. (2)], for all 22 stable alloys and 13 binary reference structures ($\Delta E_{decomp} \leq 0.0$ eV/H_2 and $\Delta E_{alloy} \leq 0.0$ eV/f.u.). References to experimental observations: !: Ref. 25, @: Ref. 37, &: Ref. 38, *: Ref. 39. Colors: Li (red), Na (blue), K (green), and reference structures (black). Labels: "MB_x" refers to "$M(BH_4)_x$." Preferred local coordination: tetra ($\square$), octa ($\bigcirc$), octa-tetra ($\triangle$), tetra-octa (+), tetra-tri ($\curlyvee$), other ($\triangleleft$).
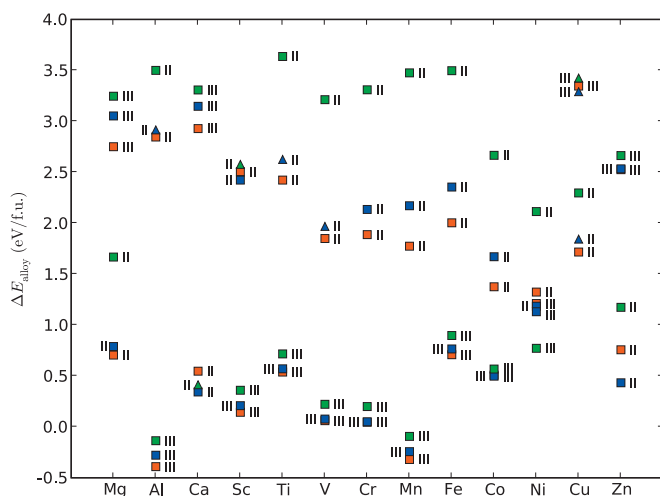
FIG. 7. The alloying energy, ΔE_{alloy}, for the 3d-metals (plus Mg, Al, and Ca) in their preferred $M_1M_2(BH_4)_x$ template structures with M_1, M_2, and B fixed for both $x=3$ and $x=4$. Colors: Li (red), Na (blue), and K (green). Preferred local coordination: tetra (□), octa (○), octa-tetra (△), tetra-octa (+). The labels indicate the oxidation state of M_2.
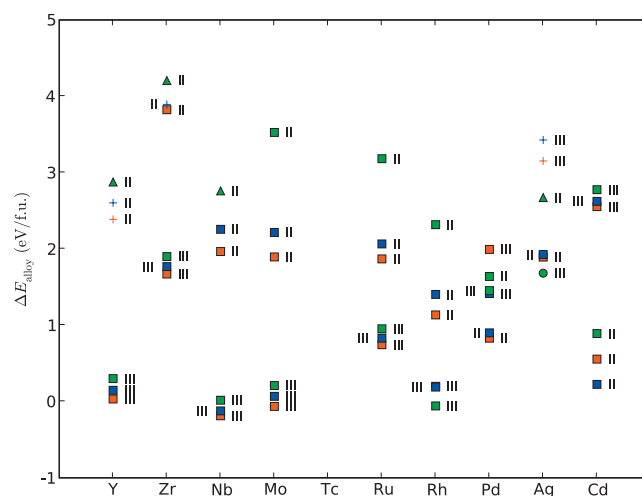

FIG. 8. The alloying energy, ΔE_{alloy}, for the 4d-metals in their preferred $M_1M_2(BH_4)_x$ template structures with M_1, M_2, and B fixed for both $x=3$ and 4. Colors: Li (red), Na (blue), and K (green). Preferred local coordination: tetra (□), octa (○), octa-tetra (△), tetra-octa (+). The labels indicate the oxidation state of M_2.

very recently or historically (circled in Figs. 5 and 6). Of the experimentally observed stable/metastable structures, LiSc(BH$_4$)$_4$,[10] KNa(BH$_4$)$_2$,[32] and Li$_2$Cd(BH$_4$)$_4$ (Ref. 30) show a weak preference for phase separation, but are all found to be potentially stable (see Table III); only LiK(BH$_4$)$_2$ (Ref. 33) ($\Delta E_{\text{alloy}}=0.202$ eV/f.u. and $\Delta E_{\text{decomp}}=-0.645$ eV/H$_2$) and LiNi(BH$_4$)$_3$ (Ref. 30) ($\Delta E_{\text{alloy}}=-0.104$ eV/f.u. and $\Delta E_{\text{decomp}}=0.069$ eV/H$_2$) fall marginally outside the selection criteria. Furthermore, LiMn(BH$_4$)$_3$ and NaMn(BH$_4$)$_3$ are found experimentally to decompose at ~100 and $110\,°\text{C}$,[34] and LiZn(BH$_4$)$_3$ and LiAl(BH$_4$)$_4$ are found to disproportionate at $\sim130\,°\text{C}$.[25] These are all structures that are located near the optimal stability in the figure (the nonshaded region).

VI. TRENDS

Given the systematic approach to the screening study it is also possible to extract information from the database about possible trends and correlations, in order to search for predictors and descriptors[35] for the design of future quaternary alloys or alloys with different cation stoichiometries.

A. 3d and 4d transition metals

The stability of the alloys, as produced by the most stable $x=3$ and $x=4$ initial template structures before the free relaxation, is presented for all 3d transition metals (plus Mg, Ca, and Al) in Fig. 7, and for the 4d transition metals in Fig. 8. A clear preference for the $M_1M_2(BH_4)_4$-tetra template is observed, which is somewhat surprising, because many of the transition metals have an oxidation state of II in the reference calculations (see Table I). This apparent discrepancy could result from partially non-ionic bonding in these structures, meaning that the coordination of the hydrogen atoms to the metal is the determining factor, not whether the metal has the "correct" valence. For instance, we find no significant energy difference between Fe$_2$(BH$_4$)$_3$ and Fe(BH$_4$)$_2$ as long as the H atoms are octahedrally coordinated to the Fe atom.

Size effects also become apparent here since the $M_1M_2(BH_4)_4$-tetra template is the only template structure that allows the coordination polyhedra of M_1 and M_2 to be relaxed independently. This is supported by the larger spacing between most of the Li, Na, and K alloy energies produced by the other template structures (see Figs. 7 and 8).

To investigate this further, the $M_1M_2(BH_4)_3$-tetra/tri-template was applied to all alloys, and in Figs. 9 and 10, the final alloy stabilities are presented; these also include the free relaxation and the additional $x=2$ and $x=5$ calculations. It is seen that the $M_1M_2(BH_4)_3$-tetra/tri-structures now become the most stable for a number of alloys and that the Li, Na, and K points lie closer indicating a reduction in the size effects.

There is a general agreement between valencies in the reference calculations and the alloys; divalent metals are
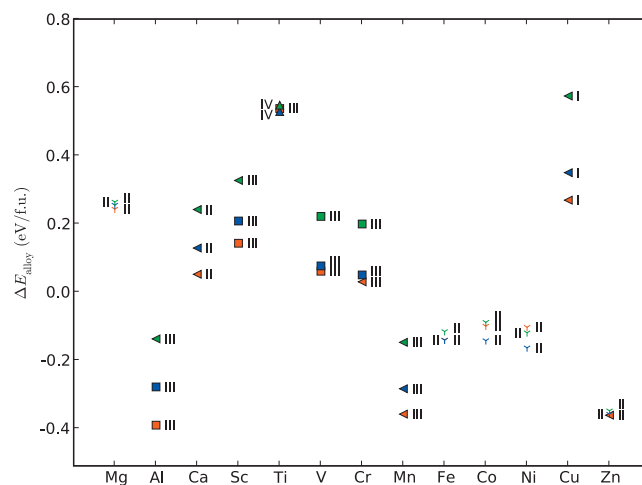

FIG. 9. The alloying energy, ΔE_{alloy}, for the 3d-metals using only the energy of the preferred $M_1M_2(BH_4)_x$, $x=2-5$ structure. Colors: Li (red), Na (blue), and K (green). Preferred local coordination: tetra (□), octa (○), octa-tetra (△), tetra-octa (+), tetra-tri (⅄), other (◁). The labels indicate the oxidation state of M_2.
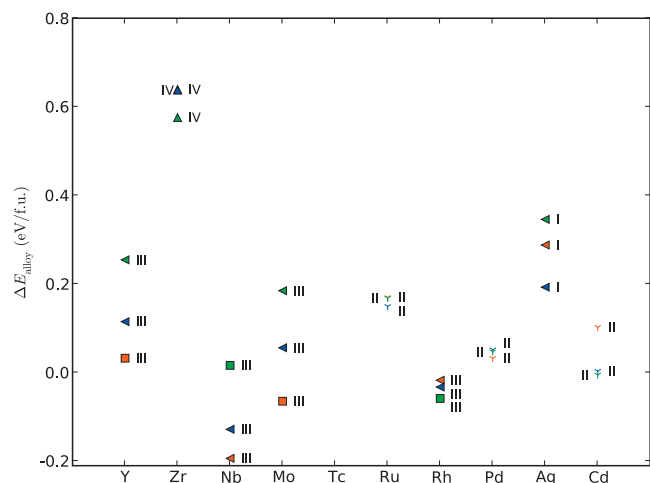
FIG. 10. The alloying energy, ΔE_{alloy}, for the 4d-metals using only the energy of the preferred $M_1M_2(BH_4)_x$, $x=2-5$ structure. Colors: Li (red), Na (blue), and K (green). Preferred local coordination: tetra (□), octa (○), octa-tetra (△), tetra-octa (+), tetra-tri (⅄), other (◁). The labels indicate the oxidation state of M_2.

FIG. 11. The decomposition energy, ΔE_{decomp}, as a function of the average Pauling electronegativity for all alloys in their preferred $M_1M_2(BH_4)_x$ coordination: tetra (□), octa (○), octa-tetra (△), tetra-octa (+), tetra-tri (⅄), other (◁). Colors: Li (red), Na (blue), and K (green).

found to prefer a $M_1M_2(BH_4)_3$ configuration, whereas trivalent metals prefer $M_1M_2(BH_4)_4$, tetravalent metals prefer $M_1M_2(BH_4)_5$ and the monovalent Cu and Ag prefer $M_1M_2(BH_4)_2$. Some deviations are found, but given the simple model structures used for both alloys and reference calculations, and given the fact that some of the metals are found by experiments to form ternary borohydrides in different oxidation states, the agreement is good.

The most stable alloys are found for the half-filled d-bands, but interesting alloys are also found for the empty and fully occupied d-bands with the addition of Al, where the $M_1Al(BH_4)_4$ are found to be promising (see Figs. 9 and 10).

Lithium-based alloys (red) are generally found to be the most stable, followed by sodium (blue) and potassium (green), although significant deviations are observed. This follows the observed trend for the storage capacities.

B. Stability versus electronegativity

A number of recent publications[33,36] have shown an apparent linear correlation between the decomposition temperature and the average cation Pauling electronegativity. Although this might be expected, given the definition of Pauling's electronegativity, it also indicates that the kinetic barriers—if any—do not appear to be particularly system dependent.

Plotting the calculated decomposition energy as a function of the average cation electronegativity for all alloys in their most stable local coordination (see Fig. 11) appears to support this observation. The scatter of the data points around the "line" (which would have a slope that agrees with Ref. 36 to within 10%–15%) is, however, significant and deviations of ± 0.1 eV/H_2 can be sufficient to shift a material from interesting to irrelevant for storage applications, or vice versa.

The stable alloys ($\Delta E_{\text{alloy}} \leq 0.0$ eV/f.u.) are seen to cluster around certain average electronegativities of 1.3–1.4 and 1.6 (see Fig. 12). The cluster around 1.3–1.4 is highly
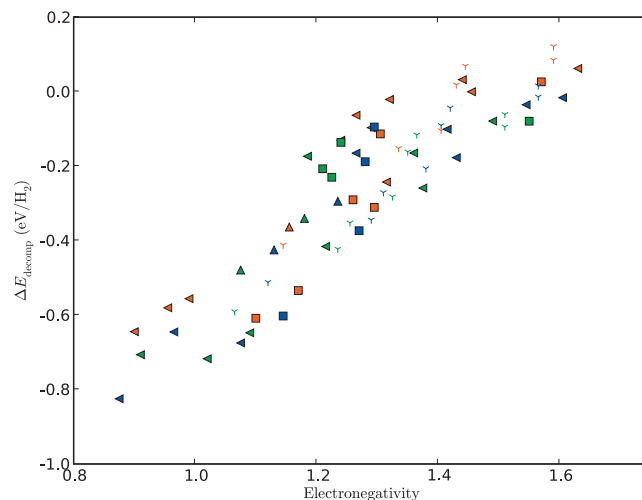
promising with $\Delta E_{\text{decomp}} \simeq -0.1$ eV/H_2 for Mn and Nb and particularly promising for Al, Zn, and Fe with $\Delta E_{\text{decomp}} \simeq -0.3$ eV/H_2. The Mo and Rh alloys at electronegativities around 1.6 are found to border on decomposition, but experimental work by Nikels *et al.*[33] estimates the decomposition temperature of such compounds to be around 150 °C.

VII. CONCLUSIONS

We have analyzed the thermodynamic properties of possible alkali-transition metal borohydride systems, finding a number of candidates showing favorable properties.

The $M_1(Al/Mn/Fe)(BH_4)_4$, $(Li/Na)Zn(BH_4)_3$, and $(Na/K)(Ni/Co)(BH_4)_3$ alloys are found to be the most promising, followed by selected $M_1(Nb/Rh)(BH_4)_4$ alloys. These findings are in good agreement with experimental observations for LiFe(BH)$_3$,[37] LiAl(BH$_4$)$_4$,[25] $(Li/Na)Mn(BH)_{3,4}$,[38]
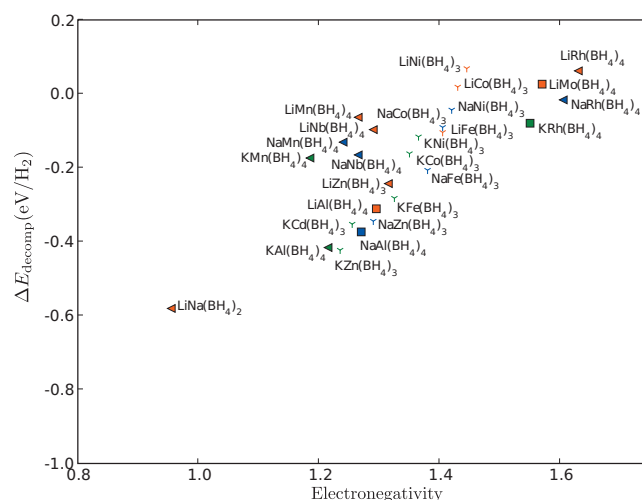

FIG. 12. The decomposition energy, ΔE_{decomp}, as a function of the average Pauling electronegativity for alloys with $\Delta E_{\text{alloy}} \leq 0.0$ eV/H_2. Colors: Li (red), Na (blue), and K (green). Preferred $M_1M_2(BH_4)_x$, $x=2-5$, coordination: tetra (■), octa (○), octa-tetra (△), tetra-octa (+), tetra-tri (⅄), other (◁).

and $(Li/Na)Zn(BH_4)_3$,[39] whereas the Co, Cd, Nb, and Rh and alloys still remain to be synthesized and tested. Although some structures can be observed experimentally in different metal-metal stoichiometries than those used in the screening study, e.g., the Li–Zn system,[39] the alloy systems were still identified as promising candidates in this screening study. Some of the nearly stable compounds in Table III, e.g., $LiSc(BH_4)_4$ (Ref. 10) and $KNa(BH_4)_2$ (Ref. 32) have recently been found to be metastable, while $LiNi(BH_4)_3$ (Ref. 30) was found to be marginally unstable here. The LCS approach was found to limit the 757 potential alloys to 22 promising candidates of which ∼10 are highly promising. These structures can now be pursued further, analyzing their detailed decomposition pathways, both theoretically[40] and experimentally.

ACKNOWLEDGMENTS

[1] L. Schlapbach and A. Züttel, Nature **414**, 353 (2001).
[2] D. Mosher, X. Tang, and S. Arsenault, DoE Hydrogen Program, FY 2006 Annual Progress Report, 2006, pp. 281–284.
[3] See http://www1.eere.energy.gov/vehiclesandfuels/about/partnerships/freedomcar/fc_goals.html for FreedomCAR and Fuel Technical Partnership Technical Goals.
[4] S. Orimo, Y. Nakamori, J. R. Eliseo, A. Züttel, and C. M. Jensen, Chem. Rev. **107**, 4111 (2007).
[5] R. Z. Sørensen, J. S. Hummelshøj, A. Klerke, J. B. Reves, T. Vegge, J. K. Nørskov, and C. H. Christensen, J. Am. Chem. Soc. **130**, 8660 (2008).
[6] A. Züttel, S. Rentsch, P. Fischer, P. Wenger, P. Sudan, P. Mauron, and C. Emmenegger, J. Alloys Compd. **356–357**, 515 (2003).
[7] Z. Łodziana and T. Vegge, Phys. Rev. Lett. **93**, 145501 (2004).
[8] Z. Łodziana and T. Vegge, Phys. Rev. Lett. **97**, 119602 (2006).
[9] K. Chłopek, C. Frommen, A. Léon, O. Zabara, and M. Fichtner, J. Mater. Chem. **17**, 3496 (2007).
[10] H. Hagemann, M. Longhini, J. W. Kaminski, T. A. Wesolowski, R. Cerný, N. Penin, M. H. Sørby, B. C. Hauback, G. Severa, and C. M. Jensen, J. Phys. Chem. A **112**, 7551 (2008).
[11] S. V. Alapati, J. K. Johnson, and D. S. Sholl, J. Phys. Chem. C **112**, 5258 (2008).
[12] V. Ozolins, E. H. Majzoub, and C. Wolverton, Phys. Rev. Lett. **100**, 135501 (2008).
[13] J. Voss, J. S. Hummelshøj, Z. Łodziana, and T. Vegge, J. Phys.: Condens. Matter **21**, 012203 (2009).
[14] P. Hohenberg and W. Kohn, Phys. Rev. **136**, B864 (1964).
[15] B. Hammer, L. B. Hansen, and J. K. Nørskov, Phys. Rev. B **59**, 7413 (1999).
[16] D. Vanderbilt, Phys. Rev. B **41**, 7892 (1990).
[17] S. R. Bahn and K. W. Jacobsen, Comput. Sci. Eng. **4**, 56 (2002).
[18] D. F. Shanno, Math. Comput. **24**, 647 (1970).
[19] F. Buchter, Z. Łodziana, A. Remhof, O. Friedrichs, A. Borgschulte, Ph. Mauron, A. Züttel, D. Sheptyakov, G. Barkhordarian, R. Bormann, K. Chłopek, M. Fichtner, M. Sørby, M. Riktor, B. Hauback, and S. Orimo, J. Phys. Chem. B **112**, 8042 (2008).
[20] See http://www.python.org for Python Programming Language.
[21] See http://subversion.tigris.org for Subversion version control system.
[22] See http://matplotlib.sourceforge.net for Matplotlib 2D plotting library for Python.
[23] J.-H. Her, M. Yousufuddin, W. Zhou, S. S. Jalisatgi, J. G. Kulleck, J. A. Zan, S.-J. Hwang, R. C. Bowman, Jr., and T. J. Udovic, Inorg. Chem. **47**, 9757 (2008).
[24] N. Hanada, K. Chłopek, C. Frommen, W. Lohstroh, and M. Fichtner, J. Mater. Chem. **18**, 2611 (2008).
[25] H.-W. Li, S. Orimo, Y. Nakamori, K. Miwa, N. Ohba, S. Towata, and A. Züttel, J. Alloys Compd. **446–447**, 315 (2007).
[26] E. Wiberg, Angew. Chem. **65**, 16 (1953).
[27] X. B. Yu, D. M. Grant, and G. S. Walker, Chem. Commun. (Cambridge) **37**, 3906 (2006).
[28] S.-J. Hwang, R. C. Bowman, Jr., J. W. Reiter, J. Rijssenbeek, G. L. Soloveichik, J.-C. Zhao, H. Kabbour, and C. C. Ahn, J. Phys. Chem. C **112**, 3164 (2008).
[29] Y. Nakamori, H.-W. Li, M. Matsuo, K. Miwa, S. Towata, and S. Orimo, J. Phys. Chem. Solids **69**, 2292 (2008).
[30] Y. Nakamori and S. Orimo, in *Solid-state Hydrogen Storage—Materials and Chemistry*, edited by G. Walker (Woodhead, Cambridge, 2008), pp. 420–449.
[31] P. Mauron, F. Buchter, O. Friedrichs, A. Remhof, M. Bielmann, C. N. Zwicky, and A. Züttel, J. Phys. Chem. B **112**, 906 (2008).
[32] L. Seballos, J. Z. Zhang, E. Ronnebro, J. L. Herberg, and E. H. Majzoub, J. Alloys Compd. **476**, 446 (2009).
[33] E. A. Nickels, M. O. Jones, W. I. F. David, S. R. Johnson, R. L. Lowton, M. Sommariva, and P. P. Edwards, Angew. Chem., Int. Ed. **47**, 2817 (2008).
[34] See http://www.docstoc.com/docs/922287/Fundamental-Studies-of-Advanced-High-Capacity-Reversible-Metal-Hydrides for "Fundamental Studies of Advanced High-Capacity, Reversible Metal Hydrides," presentation by C. M. Jensen, DOE Hydrogen Program, 13 May 2007.
[35] F. Studt, F. Abild-Pedersen, T. Bligaard, R. Z. Sørensen, C. H. Christensen, and J. K. Nørskov, Science **320**, 1320 (2008).
[36] Y. Nakamori, K. Miwa, A. Ninomiya, H. Li, N. Ohba, S. Towata, A. Züttel, and S. Orimo, Phys. Rev. B **74**, 045126 (2006).
[37] H. Nöth and P. Fritz, Angew. Chem. **73**, 408 (1961).
[38] See http://www.hydrogen.energy.gov/pdfs/review08/st_0_satyapal.pdf for "Hydrogen Storage," presentation by S. Satyapal, 2008 DOE Hydrogen Program, Merit Review and Peer Evaluation Meeting, 9 June 2008.
[39] H. Nöth, E. Wiberg, and L. Winter, Z. Anorg. Allg. Chem. **386**, 73 (1971).
[40] V. Ozolins, E. H. Majzoub, and C. Wolverton, J. Am. Chem. Soc. **131**, 230 (2009).
[41] See EPAPS Document No. E-JCPSA6-130-043923 for a listing of the authors' affiliations. For more information on EPAPS, see http://www.aip.org/pubservs/epaps.html.